Computers in Biology and Medicine 104 (2019) 81–86

Contents lists available at ScienceDirect

Computers in Biology and Medicine

journal homepage: www.elsevier.com/locate/compbiomed

Cardiac sarcoidosis classification with deep convolutional neural network-based features using polar maps☆

Ren Togo[a,1], Kenji Hirata[b], Osamu Manabe[b,*], Hiroshi Ohira[c], Ichizo Tsujino[c], Keiichi Magota[d], Takahiro Ogawa[a], Miki Haseyama[a], Tohru Shiga[b]

[a] Graduate School of Information Science and Technology, Hokkaido University, Hokkaido, 060-0814, Japan
[b] Department of Nuclear Medicine, Hokkaido University Graduate School of Medicine, Hokkaido, 060-8638, Japan
[c] First Department of Medicine, Hokkaido University Hospital, Hokkaido, 060-8638, Japan
[d] Division of Medical Imaging and Technology, Hokkaido University Hospital, Hokkaido, 060-8638, Japan

ARTICLE INFO

Keywords:
Deep learning
Convolutional neural network (CNN)
Cardiac sarcoidosis (CS)
^{18}F-FDG PET
Computer-aided diagnosis
Radiology
Machine learning
Feature extraction
Feature selection

ABSTRACT

Aims: The aim of this study was to determine whether deep convolutional neural network (DCNN)-based features can represent the difference between cardiac sarcoidosis (CS) and non-CS using polar maps.
Methods: A total of 85 patients (33 CS patients and 52 non-CS patients) were analyzed as our study subjects. One radiologist reviewed PET/CT images and defined the left ventricle region for the construction of polar maps. We extracted high-level features from the polar maps through the Inception-v3 network and evaluated their effectiveness by applying them to a CS classification task. Then we introduced the ReliefF algorithm in our method. The standardized uptake value (SUV)-based classification method and the coefficient of variance (CoV)-based classification method were used as comparative methods.
Results: Sensitivity, specificity and the harmonic mean of sensitivity and specificity of our method with the ReliefF algorithm were 0.839, 0.870 and 0.854, respectively. Those of the SUVmax-based classification method were 0.468, 0.710 and 0.564, respectively, and those of the CoV-based classification method were 0.655, 0.750 and 0.699, respectively.
Conclusion: The DCNN-based high-level features may be more effective than low-level features used in conventional quantitative analysis methods for CS classification.

1. Introduction

Cardiac sarcoidosis (CS) can cause complete heart block, ventricular or atrial arrhythmias, congestive heart failure, and sudden cardiac death [1,2]. The incidence of CS varies according to ethnicity, sex, and regions. The international Heart Rhythm Society (HRS) published a consensus statement on the diagnosis and management of CS [2,3]. The statement proposed that uptake in cardiac ^{18}F-fluorodeoxyglucose (^{18}F-FDG) positron emission tomography (PET) is one of the criteria for diagnosis of CS as is the case in the Japanese Society of Sarcoidosis and other Granulomatous Disorders (JSSOG) criteria [4]. Therefore, ^{18}F-FDG PET plays an important role in the assessment of CS [5,6] and it has been widely studied. ^{18}F-FDG uptake patterns are conventionally divided visually into the following four groups: (i) without myocardial ^{18}F-FDG uptake, (ii) definite diffuse uptake in the entire left ventricular (LV) wall, (iii) focal ^{18}F-FDG uptake, and (iv) focal of diffuse ^{18}F-FDG uptake in the left ventricular wall [7]. In these groups, group (ii) is considered to be physiological and does not indicate an abnormality, and groups (iii) and (iv) are considered to be positive for CS [8]. However, it was reported that the interobserver agreement of cardiac ^{18}F-FDG uptake image patterns was not high [9], and quantitative uptake evaluation methods are desired.

There are several conventional quantitative approaches to evaluate ^{18}F-FDG uptake for the diagnosis and management of CS using various factors such as standardized uptake value (SUV) [10], cardiac metabolic volume [11], and cardiac metabolic activity [12]. Quantitative analysis is one of the computational methods that extract the above-mentioned clinically important features for providing diagnostic

☆ **Where work was done**: Graduate School of Information Science and Technology, Hokkaido University and Department of Nuclear Medicine, Hokkaido University Graduate School of Medicine, Hokkaido University.

* Corresponding author. Department of Nuclear Medicine, Hokkaido University Graduate School of Medicine, N-15 W-7, Kita-Ku, Sapporo, 060-8638, Japan.
E-mail addresses: togo@lmd.ist.hokudai.ac.jp (R. Togo), osamumanabe817@med.hokudai.ac.jp (O. Manabe).
[1] Graduate School of Information Science and Technology, Hokkaido University, N-14, W-9, Kita-Ku, Sapporo, 060–0814, Japan.

https://doi.org/10.1016/j.compbiomed.2018.11.008
Received 24 August 2018; Received in revised form 20 October 2018; Accepted 10 November 2018

Abbreviations

CoV	coefficient of variation
CS	cardiac sarcoidosis
DCNN	deep convolutional neural network
FDG	fluorodeoxyglucose
JSSOG	Japanese society of sarcoidosis and other granulomatous disorders
LCD	low carbohydrate diet
LV	left ventricle
PET	positron emission tomography
SUV	standardized uptake value
SVM	support vector machine

supporting information [13,14]. Conventional studies have focused only on low-level features [15] that can represent simple textual patterns and distributions of images. However, semi-automated CS classification has not yet been realized since high-level semantic CS features cannot be captured.

Deep learning-based approaches may overcome the problem of feature representations. Deep learning is one of the machine learning methods that enable the input data to be related to teaching data without being explicitly programmed [16]. The basic architecture of deep leaning is inspired by the biological mechanism of the human visual attention system. In the field of medical image analysis, deep learning has shown high recognition performance for classification tasks of disease presence/absence [17]. A deep convolutional neural network (DCNN), one of representative deep learning-based methods, has already become the first-choice model for a semi-automated disease classification task [18]. In contrast to conventional low-level features, DCNN-based features that are extracted from an intermediate layer of their networks have high-level semantic information. These high-level features have high versatility for object recognition tasks [19]. DCNN-based features have been used for various automated classification tasks in the field of medical image analysis [20], and they may be useful for evaluation of CS/non-CS in ^{18}F-FDG PET.

The aim of this study was to determine whether DCNN-based features can represent CS/non-CS differences from polar maps of ^{18}F-FDG PET. The classification performance was compared with the performance of SUVmax-based classification and that of coefficient of variance (CoV)-based classification. In the proposed method, we combined DCNN-based features and a classical support vector machine (SVM) [21] classifier for a CS classification task. This approach is often called transfer learning and is effective when the number of available samples is small. Experimental results indicated that DCNN-based features are more effective than conventional texture analysis-based features in a CS/non-CS classification task.

2. Methods

2.1. Study subjects

In this retrospective study, we analyzed patients who underwent ^{18}F-FDG PET/CT and were diagnosed as having CS based on the Japanese Society of Sarcoidosis and Other Granulomatous disorders (JSSOG) guidelines [22] during the period from May 2010 to April 2017. Thirty-three CS patients who did not receive oral steroid treatment before ^{18}F-FDG PET/CT were allocated to a CS group. For a control group (non-CS group), 100 sequential patients who underwent ^{18}F-FDG PET/CT in 2013 were retrospectively investigated. The fasting duration was obtained from the patient interview record before ^{18}F-FDG injection. Patients who were less than 20 years of age, patients whose scan protocols were different, and patients who showed no uptake in the myocardium were excluded from our study. Consequently, 52 control patients were allocated to a non-CS group. Therefore, a total of 85 patients (33 CS patients and 52 non-CS patients) were analyzed as our study subjects. The study protocol was approved by the Ethics Committee of the Hokkaido University Graduate School of Medicine. Written informed consent was obtained before the study for the CS patients and with a waiver of the need for written informed consent for the non-CS group. No additional data are available.

2.2. ^{18}F-FDG PET/CT imaging acquisition protocol

An overview of the imaging acquisition protocol for the CS and non-CS patients is shown in Fig. 1. All CS patients fasted at least 18 h with a low-carbohydrate diet (LCD). Non-CS patients were instructed to drink only water and not to take any food for at least 6 h before the time of ^{18}F-FDG injection. Approximately 4.5 MBq/kg of ^{18}F-FDG was administered intravenously. CS and non-CS patients were scanned at sixty minutes after the administration of ^{18}F-FDG. PET/CT imaging was performed by a Biograph 64 TruePoint with TrueV (Siemens Japan, Tokyo). The acquired data sets were corrected for attenuation by low-dose CT images and were reconstructed by using a point spread function-based iterative algorithm (TrueX, Siemens) with two iterations per 21 subsets, a matrix size of 168 × 168, a voxel size of 4.1 × 4.1 × 2.0 mm, and a Gaussian filter at 4.0 mm full-width at half-maximum. The trans-axial and axial fields of views were 58.5 cm and 21.6 cm, respectively.

2.3. Generation of polar maps

One radiologist who had experience in imaging of CS thoroughly reviewed the PET/CT images and determined the ^{18}F-FDG-avid areas in the left ventricle (LV) region. In cases where myocardial uptake and non-myocardial uptake (e.g., mediastinal nodes) were observed, the non-myocardial parts were carefully removed manually. SUV was calculated as [tissue radioactivity (Bq/mL)] × [body weight (g)]/[injected

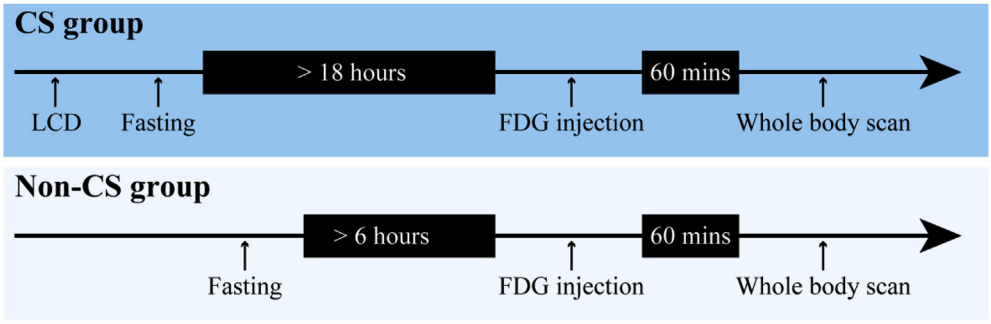

Fig. 1. ^{18}F-FDG PET/CT imaging acquisition protocol for the study subjects. CS = cardiac sarcoidosis; FDG = fluorodeoxyglucose; LCD = low-carbohydrate diet.

radioactivity (Bq)]. SUVmax was defined as the maximum value of SUV within a volume of interest. The radiologist then determined the location of the apex and angle of the axis and re-sliced the volume image to generate short-axis images. An ellipsoid model was used to approximate the LV with CT morphologic information. Short-axis slices were divided into 36 sectors, 10 degrees each [23], and a 2-dimensional polar map with a 256 × 256 matrix size was generated by a linear interpolation method.

2.4. DCNN-based CS classification method

Fig. 2 shows an overview of our newly designed DCNN-based CS classification method. For extracting high-level semantic representation features from polar maps, we used a pre-trained Inception-v3 network model [24], which is one of GoogLeNet models trained for object recognition tasks. We obtained a 2048-dimensional feature vector for each polar map, which was extracted from the *pool3* layer of the Inception-v3 network. Although the extracted high-level features can represent contents of images, these features are effective for object recognition tasks but may not be effective for CS classification tasks. In other words, the extracted features may include non-related features for CS classification. Hence, we used the ReliefF feature selection algorithm [25] to address this problem. The ReliefF algorithm is a simple and widely used approach for feature weight estimation. The weight for a feature of measurement vectors is defined in terms of feature relevance scores toward the labels of CS and non-CS. In our method, important features for the classification of CS and non-CS were automatically selected on the basis of their feature weights. Finally, a linear SVM [21] classifier was used to evaluate the effectiveness of selected DCNN-based features.

When the number of samples is small, constructing a full-scratch DCNN is difficult since DCNNs can cause over-fitting for training data. The use of a DCNN model as a feature extractor was considered to be a better way for our study.

2.5. Statistical analyses and comparative methods

The verification method was leave-one-out cross-validation. Specifically, a sample was extracted from the 85 study subjects, and the extracted sample was allocated to the test sample and the other 84 samples were allocated to training samples. We constructed the SVM classifier using those 84 training samples and estimated the label of a test sample. We repeated this step 85 times to evaluate all subjects and calculated the classification performance. The gold standard for evaluating our method was the results of reviewed ^{18}F-FDG PET/CT images. Sensitivity (= true positive/(true positive + false negative)), specificity (= true negative/(true negative + false positive)), and the harmonic mean of sensitivity and specificity (= (2 × sensitivity × specificity)/(sensitivity + specificity)) were used as evaluation criteria.

For comparison, we used SUVmax-based classification and CoV-based classification [26]. In the SUVmax-based classification, a linear SVM classifier learned the difference between SUVmax of CS patients and that of non-CS patients and classified a test sample based on the value of SUVmax. In the CoV-based classification, CoV was computed in a pixel-by-pixel manner and a linear SVM classifier learned the difference between the value of CoV in CS patients and that in non-CS patients.

For evaluation of the effectiveness of the ReliefF algorithm, we investigated the CS classification performance with change in the number of selected features based on the feature weight. Specifically, we used the top *N* (up to 2048-dimensional features for every 10-dimensional features) selected features for CS classification and calculated the classification performance.

Table 1
Characteristics of the included patients.

	CS group (n = 33)	non-CS group (n = 52)	p-value
Gender (male/female)	15/18	30/22	0.37
Age	59.0 ± 15.3	62.5 ± 13.0	0.44
Fasting time (hour)	20.4 ± 1.5	14.0 ± 3.4	< 0.0001
Fasting blood sugar (mg/dl)	89.5 ± 14.6	113.0 ± 20.3	< 0.0001
Meets JSSOG criteria	33 (100%)	0 (0%)	
Injection dose (MBq)	251.8 ± 3.4	243.7 ± 58.1	0.42

CS = cardiac sarcoidosis; JSSOG = Japanese Society of Sarcoidosis and Other Granulomatous Disorders.

3. Results

Characteristics of the CS patients and non-CS patients in this study are shown in Table 1. By our exclusion rules for the non-CS group, patients less than 20 years of age (n = 3), patients with different imaging time (n = 1), and patients without any cardiac uptake (n = 44) were excluded. Consequently, a total of 52 patients (62.5 ± 13.0 years old, 33 males) were included in the non-CS group. All of the non-CS patients suffered from a malignant disease or had been treated for a malignant disease.

The training and testing totally took ~2 min with a single NVIDIA GeForce GTX 1080 Ti GPU. Table 2 shows the classification performance of our method, that of the SUVmax-based classification method, and that of the CoV-based classification method. Sensitivity, specificity and the harmonic mean of our method with the ReliefF algorithm (with selection of 100-dimensional DCNN-based features) were 0.839, 0.870 and 0.854, respectively. Note that this was the best performance of our method. In more detail, 26 (78.8%) of the 33 CS patients were correctly classified into the CS group, and 47 (90.0%) of the 52 non-CS patients were correctly classified into the non-CS group. Examples of polar maps correctly and incorrectly classified in our method are shown in Fig. 3. The color bar represents the value of SUV. Sensitivity, specificity and the harmonic mean of our method without the ReliefF algorithm (using 2048-dimensional DCNN-based features) were slightly lower; 0.800, 0.836 and 0.818, respectively.

For comparative methods, sensitivity, specificity and the harmonic mean of the SUVmax-based classification method were 0.468, 0.710 and 0.564, respectively, and those of the CoV-based classification

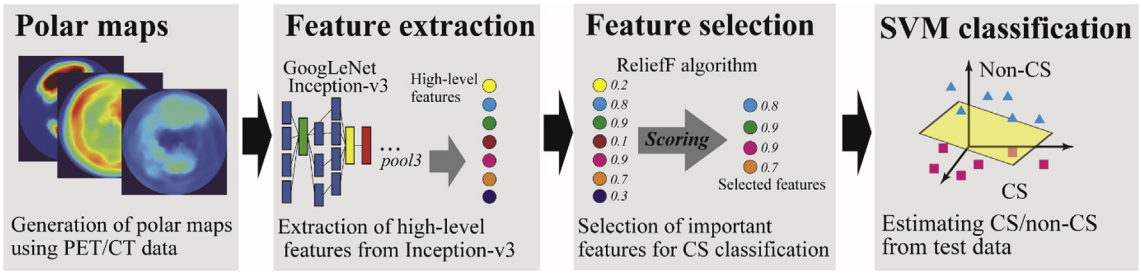

Fig. 2. Overview of our cardiac sarcoidosis (CS) detection method. SVM = support vector machine.

Table 2
Cardiac sarcoidosis (CS) detection performance results. The upper two rows show the performance of our method, and the lower two rows show the performances of comparative methods. Harmonic mean (= (2 × sensitivity × specificity)/(sensitivity + specificity)) represents the total performance of CS detection.

	Sensitivity	Specificity	Harmonic mean
Our method (With the ReliefF algorithm)	**0.839**	**0.870**	**0.854**
Our method (Without the ReliefF algorithm)	0.800	0.836	0.818
SUV-based classification	0.468	0.710	0.564
CoV-based classification	0.655	0.750	0.699

method were 0.655, 0.750 and 0.699, respectively. Experimental results showed that our DCNN-based method outperformed the conventional comparative methods.

Fig. 4 shows the results of CS classification performance by our method with change in the number of selected features. In this study, the ReliefF algorithm gave an importance score to each of the extracted DCNN-based features, and the top *N* features were used for CS classification. Overall, the harmonic mean was approximately in the range of 0.80–0.85. We confirmed that most of the DCNN-based features were effective for the CS classification task, the performance being somewhat improved with the ReliefF algorithm. On the other hand, when considering only the top 10-dimensional features, sensitivity, specificity and the harmonic mean were 0.741, 0.666 and 0.722, respectively. This performance was roughly equivalent to the performance of the CoV-based classification method.

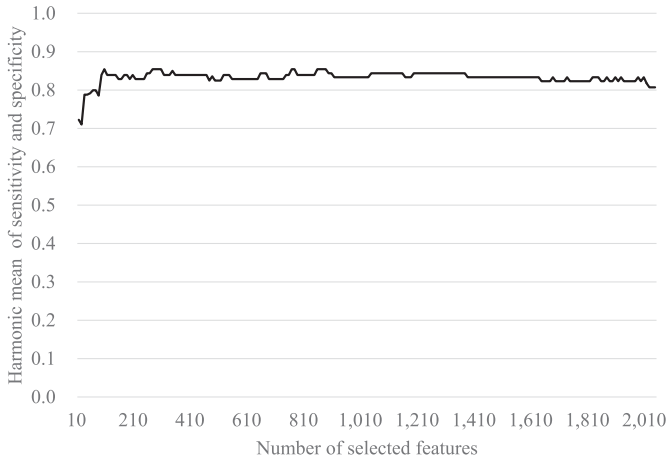

Fig. 4. Cardiac sarcoidosis (CS) detection performance with change in the number of selected features. The horizontal axis is the number of selected features by the ReliefF algorithm. The vertical axis is the harmonic mean of sensitivity and specificity that can represent the total performance of CS detection.

4. Discussion

We developed a semi-automated CS classification method for ^{18}F-FDG PET/CT and compared the classification performance of our method with the performances of SUVmax-based and CoV-based classification methods as the first step for establishing a semi-automated CS diagnosis supporting system. Full-scratch DCNN training is a popular approach for classification problems when abundant training image data can be obtained. However, a DCNN can easily fall into the overfitting problem when training samples are limited. Since the number of evaluated samples in this study was 85, a full-training CNN was not suitable for the task. Therefore, we took a transfer learning approach that uses CNN architectures as a feature extractor to confirm the effectiveness of DCNN-based features for the CS classification task. Experimental results showed that our method had the potential for realizing a semi-automated diagnosing support system for CS classification.

The most important difference between our method and comparative methods is the types of features. The Inception-v3 network used in this study is a model that achieves high recognition performance in

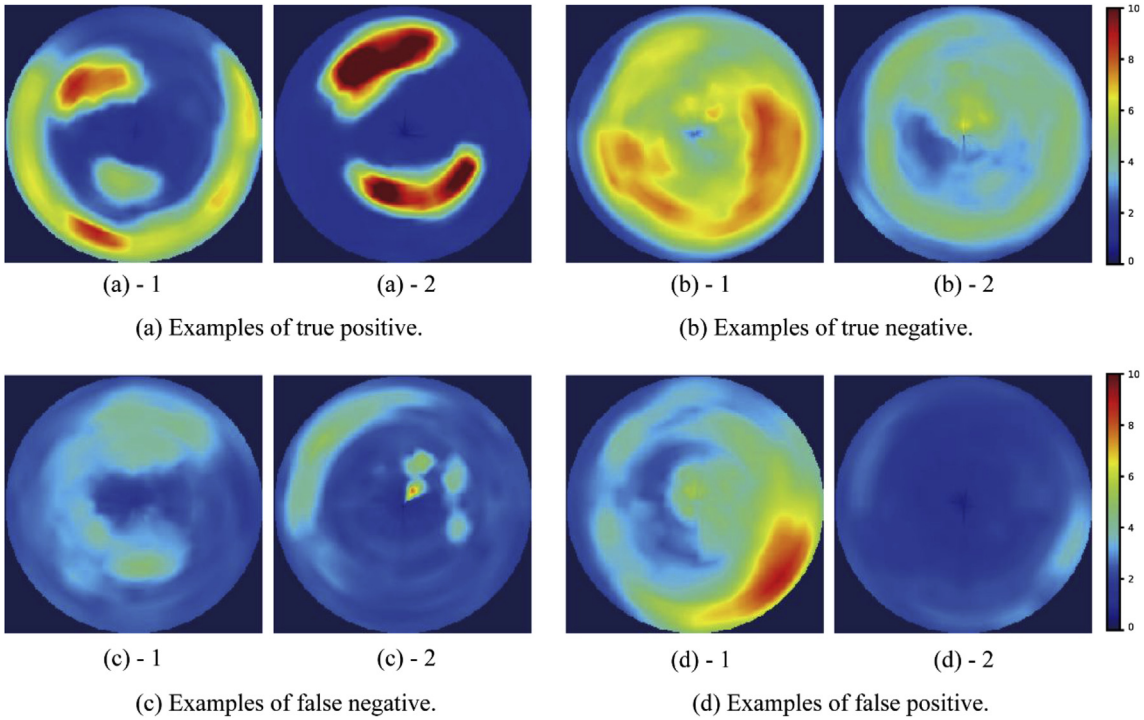

Fig. 3. Examples of polar maps correctly and incorrectly classified in our method: (a) examples of true positive, (b) examples of true negative, (c) examples of false negative, and (d) examples of false positive. The color bar represents the standardized uptake value (SUV).

object recognition tasks. Specifically, Inception-v3 network was trained for ImageNet Large Visual Recognition Challenge [27]. In this competition task, constructed models were used to classify various images into 1000 classes including “Zebra”, “Leopard”, and “Dishwasher”. The Inception-v3 network achieved a 3.46% top-5 error rate in that task. This means that the trained Inception-v3 network can produce sophisticated high-level semantic features. We developed a CS classification method utilizing these high-level semantic features. On the other hand, SUVmax reflects a single voxel value and that does not account for the metabolism of the entire distribution of a target lesion. Also, CoV is calculated with a standard deviation and an arithmetical mean. However, SUVmax and CoV are still low-level features compared to DCNN-based features. Experimental results suggested that high-level features extracted from the Inception-v3 network are better than the features in other methods for capturing characteristics of CS and non-CS.

The other contribution of our study is evaluation of the effectiveness of using a feature selection algorithm. When radiologists diagnose CS, they consider many factors such as SUVmax, variation of SUV, and uptake location. Then factors that are non-related to CS and non-CS are ignored [28]. In order to use an approach that is similar role to this approach, we applied a simple feature selection method to DCNN-based features for improving CS classification performance. Experimental results showed the effectiveness of the feature selection algorithm. This suggested that features extracted from the Inception-v3 network include some non-related features for CS classification.

In the assessment of CS, physiological ^{18}F-FDG uptake sometimes causes false positive and false negative results or difficulties in the assessment [29]. In the most common classification, ^{18}F-FDG uptake patterns in the LV wall are divided into four groups based on visual analyses: (i) lack of myocardial ^{18}F-FDG uptake, (ii) definite diffuse uptake in the entire LV wall, (iii) focal uptake, and (iv) focal or diffuse ^{18}F-FDG uptake [7]. Morooka et al. reported that diffuse uptake or basal ring-like and/or lateral uptake was observed as the physiological pattern in patients with suspected or known CS [30]. The interobserver agreement of cardiac ^{18}F-FDG uptake image patterns was not high [31]. Several methods to reduce physiological myocardial ^{18}F-FDG uptake, such as long fasting, low-carbohydrate/high-fat food intake and unfractionated heparin injection prior to ^{18}F-FDG administration, have been proposed. The interobserver agreement was better in patients who received such preparation [31]. However, it is still difficult to distinguish active inflammation and physiological ^{18}F-FDG uptake in some patients. With the development of computing technology in recent years, deep learning techniques have already indicated the possibility of being a reference for radiologists in various diseases [32,33]. The present study is a preliminary study on the effectiveness of deep learning techniques in the field of cardiac imaging for reducing the burden of radiologists.

There are several methodological limitations in this study. First, all of the patients were scanned without respiratory or electrocardiogram gating. Although respiratory and cardiac motions may affect a polar map reconstruction procedure, their effects were not investigated. Second, fasting for more than 18 h combined with a low-carbohydrate diet is the standard preparation in our institute to reduce physiological LV ^{18}F-FDG uptake for assessment of cardiac sarcoidosis (23). Therefore, the fasting time was longer for the CS group than for non-CS group in this study. Finally, our newly developed method was evaluated using data from a single center. Evaluation using data from multiple centers would provide more accurate results of DCNN-based features. Also, since the number of evaluated samples in this study was relatively small, we used a DCNN model as a feature extractor. Full-scratch DNN evaluation with a large-scale ^{18}F-FDG PET dataset is one of our future works.

Disclosure

None declared.

Acknowledgement

This study was partly supported by Global Station for Big Data and Cybersecurity at Hokkaido University, the Center of Innovation Program from Japan Science and Technology Agency Grant Number H30W16, and JSPS KAKENHI Grant Number JP17H01744.

References

[1] R. Kandolin, J. Lehtonen, M. Kupari, Cardiac sarcoidosis and giant cell myocarditis as causes of atrioventricular block in young and middle-aged adults, Circ. Arrhythmia Electrophysiol. 4 (2011) 303–309, https://doi.org/10.1161/CIRCEP.110.959254.

[2] N.R. Aggarwal, D. Snipelisky, P.M. Young, B.J. Gersh, L.T. Cooper, P. Chareonthaitawee, Advances in imaging for diagnosis and management of cardiac sarcoidosis, Eur. Hear. J. - Cardiovasc. Imaging. 16 (2015) 949–958, https://doi.org/10.1093/ehjci/jev142.

[3] D.H. Birnie, W.H. Sauer, F. Bogun, J.M. Cooper, D.A. Culver, C.S. Duvernoy, M.A. Judson, J. Kron, D. Mehta, J. Cosedis Nielsen, A.R. Patel, T. Ohe, P. Raatikainen, K. Soejima, HRS expert consensus statement on the diagnosis and management of arrhythmias associated with cardiac sarcoidosis, Heart Rhythm 11 (2014) 1305–1323, https://doi.org/10.1016/j.hrthm.2014.03.043.

[4] O. Manabe, M. Naya, K. Yoshinaga, N. Oyama-Manabe, H. Ohira, T. Aikawa, N. Tamaki, Assessment of myocardial blood flow and cardiac FDG uptake using positron emission tomography, Ann. Nucl. Cardiol. 3 (2017) 205–209, https://doi.org/10.17996/anc.17-00014.

[5] G. Youssef, E. Leung, I. Mylonas, P. Nery, K. Williams, G. Wisenberg, K.Y. Gulenchyn, R.A. deKemp, J. DaSilva, D. Birnie, G.A. Wells, R.S.B. Beanlands, The use of 18F-FDG PET in the diagnosis of cardiac sarcoidosis: a systematic review and metaanalysis including the Ontario experience, J. Nucl. Med. 53 (2012) 241–248, https://doi.org/10.2967/jnumed.111.090662.

[6] R. Langah, K. Spicer, M. Gebregziabher, L. Gordon, Effectiveness of prolonged fasting 18f-FDG PET-CT in the detection of cardiac sarcoidosis, J. Nucl. Cardiol. 16 (2009) 801–810, https://doi.org/10.1007/s12350-009-9110-0.

[7] M. Miyagawa, R. Tashiro, E. Watanabe, N. Kawaguchi, H. Ishimura, T. Kido, T. Kido, A. Kurata, T. Mochizuki, Optimal Patient Preparation for Detection and Assessment of Cardiac Sarcoidosis by FDG-PET, (n.d.). doi:10.17996/anc.17-00037.

[8] K. Yoshinaga, O. Manabe, H. Ohira, N. Tamaki, Focus issue on cardiac sarcoidosis from international congress of nuclear cardiology and cardiac CT (ICNC 12) symposium, Ann. Nucl. Cardiol, Japanese Society of Nuclear Cardiology, 2015, pp. 87–94, , https://doi.org/10.17996/ANC.01.01.87.

[9] H. Ohira, B.M. Ardle, R.A. deKemp, P. Nery, D. Juneau, J.M. Renaud, R. Klein, O. Clarkin, K. MacDonald, E. Leung, G. Nair, R. Beanlands, D. Birnie, Inter- and intraobserver agreement of 18F-FDG PET/CT image interpretation in patients referred for assessment of cardiac sarcoidosis, J. Nucl. Med. 58 (2017) 1324–1329, https://doi.org/10.2967/jnumed.116.187203.

[10] E. Gontier, E. Fourme, M. Wartski, C. Blondet, G. Bonardel, E. Le Stanc, M. Mantzarides, H. Foehrenbach, H. Ohira, B.M. Ardle, A. Robert, P. Nery, D. Juneau, J.M. Renaud, R. Klein, O. Clarkin, K. Macdonald, E. Leung, G. Nair, R. Beanlands, D. Birnie, R. Yokoyama, M. Miyagawa, H. Okayama, T. Inoue, H. Miki, A. Ogimoto, J. Higaki, T. Mochizuki, Quantitative analysis of myocardial ^{18}F-fluorodeoxyglucose uptake by PET/CT for detection of cardiac sarcoidosis, Int. J. Cardiol. 195 (2015) 180–187, https://doi.org/10.1016/j.ijcard.2015.05.075.

[11] R.J. Francis, M.J. Byrne, A. a van der Schaaf, J. a Boucek, A.K. Nowak, M. Phillips, R. Price, A.P. Patrikeos, a W. Musk, M.J. Millward, Early prediction of response to chemotherapy and survival in malignant pleural mesothelioma using a novel semiautomated 3-dimensional volume-based analysis of serial 18F-FDG PET scans, J. Nucl. Med. 48 (2007) 1449–1458, https://doi.org/10.2967/jnumed.107.042333.

[12] A. Ahmadian, A. Brogan, J. Berman, A.L. Sverdlov, G. Mercier, M. Mazzini, P. Govender, F.L. Ruberg, E.J. Miller, Quantitative interpretation of FDG PET/CT with myocardial perfusion imaging increases diagnostic information in the evaluation of cardiac sarcoidosis, J. Nucl. Cardiol. 21 (2014) 925–939, https://doi.org/10.1007/s12350-014-9901-9.

[13] P.A. Calvert, D.R. Obaid, M.O. Sullivan, L.M. Shapiro, D. Mcnab, C.G. Densem, P.M. Schofield, D. Braganza, S.C. Clarke, K.K. Ray, N.E.J. West, M.R. Bennett, Association between IVUS findings and adverse outcomes in patients with coronary artery disease the VIVA (VH-IVUS in vulnerable atherosclerosis) study, JCMG 4 (2011) 894–901, https://doi.org/10.1016/j.jcmg.2011.05.005.

[14] L. Wang, W. Li, Y. Yang, W. Wu, Q. Cai, X. Ma, C. Xiong, J. He, W. Fang, Quantitative assessment of right ventricular glucose metabolism in idiopathic pulmonary arterial hypertension patients: a longitudinal study, Eur. Hear. J. – Cardiovasc. Imaging. 17 (2016) 1161–1168, https://doi.org/10.1093/ehjci/jev297.

[15] D. Tezuka, M. Terashima, Y. Kato, A. Toriihara, K. Hirasawa, T. Sasaoka, S. Yoshikawa, Y. Maejima, T. Ashikaga, J.-I. Suzuki, K. Hirao, M. Isobe, Clinical characteristics of definite or suspected isolated cardiac sarcoidosis: application of cardiac magnetic resonance imaging and 18F-Fluoro-2-deoxyglucose positron-emission tomography/computerized tomography, J. Card. Fail. 21 (2015) 313–322, https://doi.org/10.1016/j.cardfail.2014.12.004.

[16] K. Yasaka, H. Akai, A. Kunimatsu, S. Kiryu, O. Abe, Deep learning with convolutional neural network in radiology, Jpn. J. Radiol. 36 (2018) 257–272, https://doi.org/10.1007/s11604-018-0726-3.

[17] Y. Lecun, Y. Bengio, G. Hinton, Deep learning, Nature 521 (2015) 436–444, https://doi.org/10.1038/nature14539.

[18] G. Litjens, T. Kooi, B.E. Bejnordi, A.A.A. Setio, F. Ciompi, M. Ghafoorian, J.A.W.M. van der Laak, B. van Ginneken, C.I. Sánchez, A survey on deep learning in medical image analysis, Med. Image Anal. 42 (2017) 60–88, https://doi.org/10.1016/j.media.2017.07.005.

[19] S.M. Erfani, S. Rajasegarar, S. Karunasekera, C. Leckie, High-dimensional and large-scale anomaly detection using a linear one-class SVM with deep learning, Pattern Recogn. 58 (2016) 121–134, https://doi.org/10.1016/J.PATCOG.2016.03.028.

[20] D. Cheng, M. Liu, Classification of alzheimer's disease by cascaded convolutional neural networks using PET images, Springer, Cham, 2017, pp. 106–113, , https://doi.org/10.1007/978-3-319-67389-9_13.

[21] C. ~Cortes, V. ~Vapnik, Support vector networks, Mach. Learn. 20 (1995) 273~–~297, https://doi.org/10.1007/BF00994018.

[22] O. Manabe, H. Ohira, K. Yoshinaga, M. Naya, N. Oyama-Manabe, N. Tamaki, Qualitative and quantitative assessments of cardiac sarcoidosis using ^{18}F-FDG PET, Ann. Nucl. Cardiol., Japanese Society of Nuclear Cardiology, 2017, pp. 117–120, , https://doi.org/10.17996/anc.17-00015.

[23] T. Journal, N. Medicine, A reverse flow-metabolism mismatch pattern on PET is related to ... J. Nucl. Med. 40 (1999) 1492.

[24] C. Szegedy, V. Vanhoucke, S. Ioffe, J. Shlens, Z. Wojna, Rethinking the inception architecture for computer vision, Proc. IEEE Conf. Comput. Vis. Pattern Recognit, 2016, pp. 2818–2826, , https://doi.org/10.1109/CVPR.2016.308.

[25] M. Robnik-Šikonja, I. Kononenko, Theoretical and empirical analysis of ReliefF and RReliefF, Mach. Learn. 53 (2003) 23–69, https://doi.org/10.1023/A:1025667309714.

[26] N. Tahara, A. Tahara, Y. Nitta, N. Kodama, M. Mizoguchi, H. Kaida, K. Baba, M. Ishibashi, N. Hayabuchi, J. Narula, T. Imaizumi, Heterogeneous myocardial FDG uptake and the disease activity in cardiac sarcoidosis, JACC Cardiovasc. Imaging 3 (2010) 1219–1228, https://doi.org/10.1016/j.jcmg.2010.09.015.

[27] A. Krizhevsky, I. Sutskever, G.E. Hinton, ImageNet classification with deep convolutional neural networks, Adv. Neural Inf. Process. Syst, 2012, pp. 1–9 https://doi.org/10.1016/j.protcy.2014.09.007.

[28] N. Kwak, Chong-Ho Choi, Input feature selection for classification problems, IEEE Trans. Neural Network. 13 (2002) 143–159, https://doi.org/10.1109/72.977291.

[29] H. Ohira, I. Tsujino, S. Ishimaru, N. Oyama, T. Takei, E. Tsukamoto, M. Miura, S. Sakaue, N. Tamaki, M. Nishimura, Myocardial imaging with 18F-fluoro-2-deoxyglucose positron emission tomography and magnetic resonance imaging in sarcoidosis, Eur. J. Nucl. Med. Mol. Imag. 35 (2008) 933–941, https://doi.org/10.1007/s00259-007-0650-8.

[30] M. Morooka, M. Moroi, K. Uno, K. Ito, J. Wu, T. Nakagawa, K. Kubota, R. Minamimoto, Y. Miyata, M. Okasaki, O. Okazaki, Y. Yamada, T. Yamaguchi, M. Hiroe, Long fasting is effective in inhibiting physiological myocardial 18 F-FDG uptake and for evaluating active lesions of cardiac sarcoidosis, (n.d.). https://ejnmmires.springeropen.com/track/pdf/10.1186/2191-219X-4-1 (accessed June 4, 2018).

[31] P.R. Vennalaganti, V. Naag Kanakadandi, S.A. Gross, S. Parasa, K.K. Wang, N. Gupta, P. Sharma, Inter-observer agreement among pathologists using wide-area transepithelial sampling with computer-assisted analysis in patients with barrett's esophagus, Am. J. Gastroenterol. 110 (2015) 1257–1260, https://doi.org/10.1038/ajg.2015.116.

[32] P. Lakhani, B. Sundaram, Deep learning at chest radiography: automated classification of pulmonary tuberculosis by using convolutional neural networks, Radiology 284 (2017) 574–582, https://doi.org/10.1148/radiol.2017162326.

[33] S. Shichijo, S. Nomura, K. Aoyama, Y. Nishikawa, M. Miura, T. Shinagawa, H. Takiyama, T. Tanimoto, S. Ishihara, K. Matsuo, T. Tada, Application of convolutional neural networks in the diagnosis of Helicobacter pylori infection based on endoscopic images, EBioMedicine 25 (2017) 106–111, https://doi.org/10.1016/j.ebiom.2017.10.014.